2020 IEEE/RSJ International Conference on Intelligent Robots and Systems (IROS)
October 25-29, 2020, Las Vegas, NV, USA (Virtual)

A frequency-dependent impedance controller for an active-macro/passive-mini robotic system

Nicolas Badeau and Clément Gosselin

Abstract— **This paper presents an alternative impedance controller for a macro-mini robotic system in which the mini robot is unactuated. The approach is verified experimentally on a simple two-degree-of-freedom macro-mini robot. The dynamic analysis of the robot is first presented. Then, a standard impedance controller is derived and analysed. Such a controller is shown to be experimentally unstable when used with the present macro-mini mechanism. An alternative impedance controller is then proposed and analysed. While slightly more complex than the standard controller, it provides a more stable behaviour experimentally. The alternative controller also increases the effectiveness of the control by reducing the response to high-frequency motion such as hand tremor.**

I. Introduction

Physical human-robot interaction is considered as a means of allowing robots and humans to communicate safely and intuitively. This paradigm is applied in several contexts including industrial applications, human assistance and medical robotics. Several approaches have been proposed in the literature to implement such a physical interaction (see for instance [1]–[3]).

Among other possible approaches, the active-macro/passive-mini concept was proposed in previous work in order to provide an intuitive low-impedance interaction to the human user [4]–[6]. In this concept, a low-impedance passive mini robot is mounted on a high-impedance actuated macro robot. The mini robot provides the low-impedance interaction with the user and its displacement is used as an input for the motion of the active macro robot. This concept was shown to be very effective for 3-dof and 4-dof tasks in [5], [6]. In [5], a controller is developed for the macro-mini concept. The controller is based on impedance control [7]. However, the standard impedance control approach was modified in this case in order to account for the particular behaviour of the passive mini robot.

The design of this controller was inspired from other impedance and admittance controllers, which include, for example, variable impedance terms [8], friction compensation [9], complementary stability provisions [10], adaptive terms [11], [12] or robust control concepts [13].

Although a stable and effective controller for a macro-mini robot was demonstrated in [5], [6], the systematic study of the control of a macro-mini system remains a subject of interest, which may yield novel control approaches that could further improve the results obtained with such a kinematic arrangement. In particular, it can be observed that the controllers proposed so far for the macro-mini concept do not use a virtual mass linked to the mini mechanism acceleration. It will be demonstrated in this paper, using a standard impedance controller, that the virtual mass M_d term of the impedance controller causes instability of the macro-mini system. An alternative impedance control is then proposed and compared with the standard impedance controller.

This paper is structured as follows. Section II describes the simplified macro-mini mechanism architecture as well as the experimental set-up. The simplified macro-mini system's dynamics are presented in Section III. The standard impedance controller is described in Section IV together with the theoretical stability analysis and the experimental results obtained. Section V uses the same structure to present the alternative impedance controller. A brief conclusion is given in Section VI.

II. Experimental Setup

The experimental set-up used in this study includes an actuated one-degree-of-freedom (one-dof) macro component and an unactuated one-dof mini component. The macro component consists of a horizontal prismatic joint composed of a ball screw actuated by a DC motor on which a guided cart is mounted. The mini component consists of a pendulum type link mounted on a pivot attached to the cart. The pivot is connected to a backdrivable motor. This motor is only used to generate impulses for the experimental analysis: the current in the motor is always zero at any other given time and therefore the mini component of the robot can be considered passive. A photograph of the experimental setup is shown in Fig. 1. The macro motor is a RDM-103 (series 2008) from Servo Systems, the rail is from Thomson (model 2HBM100YPHL) and the encoder is a DA15-1000-5VLD (serie 256, ADC-256D) from Tamagawa. The mini mechanism motor is a Maxon DC motor with integrated encoder (model 500267).

III. Dynamic Analysis

The two-dof macro-mini system is represented schematically in Fig. 2. The macro mechanism of mass M is mounted on a rail and its displacement with respect to a fixed origin is given by $x_M(t)$. The force $F(t)$ is the macro actuator force applied on the cart. The rotation of the mini mechanism is measured by angle $\theta(t)$. The mini link length

*The financial support of the Natural Sciences and Engineering Research Council of Canada (NSERC) and of the Canada Research Chair program is gratefully acknowledged.

The authors are with the Department of Mechanical Engineering, Université Laval, Québec, Qc, Canada, nicolas.badeau@olympus.com, gosselin@gmc.ulaval.ca

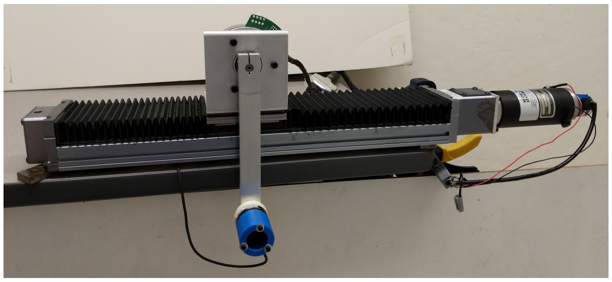

Fig. 1: Photograph of the macro-mini simplified mechanism used for the experimental test.

is noted l and its mass (considered a point mass) is noted m. The gravitational acceleration is noted g and the velocity of mass m is given by $\vec{v}_m(t)$. An external force $\vec{f}_h(t)$ is applied to the mini mechanism by the user. The torque $\tau_c(t)$ represents the possible torque that can be applied by the motor of the mini mechanism. However, in this paper, this torque is considered to be zero at any given time ($\tau_c(t) = 0$).

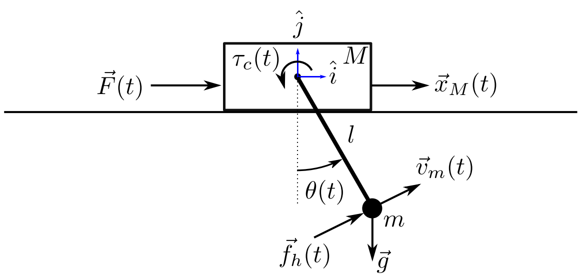

Fig. 2: Schematic of the active-macro/passive-mini robotic mechanism.

The dynamic model of the two-dof system is readily obtained using any general dynamic analysis approach. One obtains the following equations of motion

$$F(t) = (M+m)\ddot{x}_M(t)+ml\ddot{\theta}(t)\cos(\theta(t))-ml\dot{\theta}^2(t)\sin(\theta(t)) \tag{1}$$

and

$$ml\ddot{\theta}(t) = -mg\sin(\theta(t)) - m\ddot{x}_M(t)\cos(\theta(t)) + f_h(t) \tag{2}$$

where $\ddot{x}_M(t)$ represents the acceleration of the macro mechanism.

Using the small angle approximations $\{\sin(\theta) \approx \theta;\ \cos(\theta) \approx 1\}$ and considering the angular velocity to be small $\{\dot{\theta}^2(t) \approx 0\}$, the dynamic model can be simplified to

$$F(t) = (M+m)\ddot{x}_M(t) + ml\ddot{\theta}(t) \tag{3}$$

$$ml\ddot{\theta}(t) = f_h(t) - mg\theta(t) - m\ddot{x}_M(t) \tag{4}$$

Moreover, using (4), (3) can be rewritten as

$$F(t) = f_h(t)\frac{M+m}{m} - g(M+m)\theta(t) - Ml\ddot{\theta}(t). \tag{5}$$

It should be pointed out that friction was neglected in the analysis because it is difficult to model and since a viscous term can be included in the impedance model.

IV. Standard Impedance Controller

The impedance controller aims at linking the input motion of the mini mechanism to a desired force $F(t)$ to be applied on the macro mechanism. Here, the input motion corresponds to the mini mechanism motion $\{p(t), \dot{p}(t), \ddot{p}(t)\}$ and the output corresponds to the force $F(t)$. The impedance controller equation is written as

$$F(t) = M_d\ddot{p}(t) + C_d\dot{p}(t) + K_d p(t) \tag{6}$$

where, using the small angle approximation, one has

$$p(t) = l\theta(t). \tag{7}$$

The controller equation can then be rewritten as

$$F(t) = M_d l\ddot{\theta}(t) + C_d l\dot{\theta}(t) + K_d l\theta(t). \tag{8}$$

The input current $I_M(t)$ of the DC motor is then obtained as

$$I_M(t) = \frac{\tau_M(t)}{\tau_{kM}} = \frac{\rho}{2\pi\eta\tau_{kM}}F(t) \tag{9}$$

where $\tau_M(t)$ is the motor torque, τ_{kM} is the motor torque constant, ρ is the pitch of the ball screw and η is the ball screw efficiency.

With the dynamic model (5) and the standard impedance controller (8), the system response $\theta(t)$ caused by an external perturbation $f_h(t)$ can be theoretically computed using a Laplace analysis. Equation (5) is first substituted into (8). Then, solving for the external force $f_h(t)$ and taking the Laplace transform yields the transfer function

$$H(s) = \frac{\Theta(s)}{F_H(s)} = \frac{m+M}{(M_d+M)ml}\left[\frac{1}{s^2+2\zeta\omega_0 s+\omega_0^2}\right] \tag{10}$$

with

$$\begin{aligned} \omega_0^2 &= \frac{a_0}{a_2}, \quad 2\zeta\omega_0 = \frac{a_1}{a_2} \\ a_0 &= \left(\frac{K_d}{M} + \frac{g}{l}(1+\frac{m}{M})\right) \\ a_1 &= \frac{C_d}{M}, \quad a_2 = \frac{M_d}{M}+1 \end{aligned} \tag{11}$$

where $F_H(s)$ and $\Theta(s)$ are respectively the Laplace transform of $f_h(t)$ and $\theta(t)$. The above transfer function represents a second-order low-pass filter. From (11), one has

$$\begin{aligned} \zeta &= \frac{C_d}{2\sqrt{(M_d+M)(K_d+\frac{g}{l}(m+M))}} \\ \omega_0 &= +\sqrt{\frac{K_d+\frac{g}{l}(m+M)}{M_d+M}}. \end{aligned} \tag{12}$$

Hence, the damping ratio ζ is a function of all gains while the cut-off frequency ω_0 is only a function of the virtual mass and stiffness.

A critically damped system is targeted, namely $\zeta = 1$. Also, above the cut-off frequency ω_0, the system response is decreasing linearly with the perturbation frequency. In this application, we would like to have the same response for much of the human bandwidth, hence the angular cut-off frequency must be higher than the human arm motion frequency. In order to include a safety margin, the cut-off frequency is selected as $\omega_0 = 100$ rad/s [6]. The above two conditions on ζ and ω_0 yield

$$\begin{aligned} M_d &= \frac{K_d + \frac{g}{l}(m+M)}{\omega_0^2} - M \\ C_d &= \frac{2\zeta}{\omega_0}(K_d + \frac{g}{l}(m+M)) \end{aligned} \tag{13}$$

with the following constraints, which arise from the square roots

$$\begin{aligned} K_d &\geq 0 \\ K_d &\geq M\omega_0^2 - \frac{g}{l}(m+M) \end{aligned} \tag{14}$$

where the virtual stiffness K_d is used as the free variable for the adjustment of the parameters.

Experiments were conducted in order to validate the theoretical stability analysis presented above. The method described in [5] was used to experimentally set the controller gains. In order to reliably generate a repeatable impulse on the mini mechanism, a torque impulse was sent to the mini-mechanism motor. The amplitude of the impulse is 2 A and its duration is 0.1 s. Some experimental results are shown in Fig. 3. From this figure, an appropriate domain for the virtual stiffness K_d seems to be around $[1000, 2000]$.

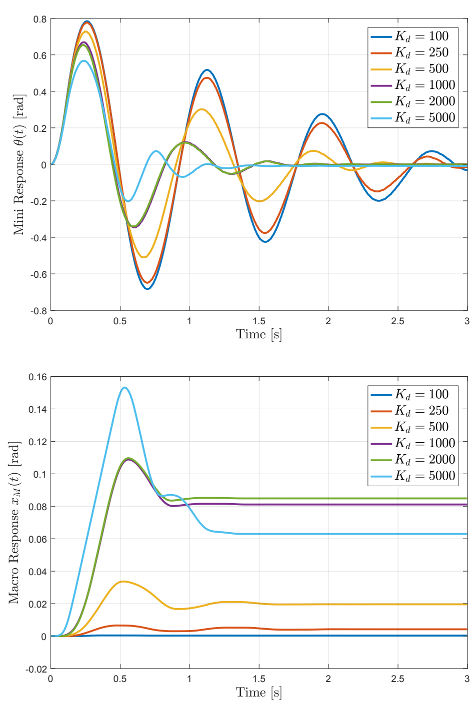

Fig. 3: Experimental response for different virtual stiffness K_d values. $\{M_d = C_d = 0\}$

Based on the experiments performed, it was observed that the virtual damping C_d should be chosen within the range $[400; 800]$ which corresponds to a theoretical damping ratio between $\zeta = 5.125$ and $\zeta = 10.25$, representing an over-damped system. A comparison of the experimental and simulated response in this case (with the gains selected as $M_d = 0$, $C_d = 400$, $K_d = 1000$ shows that the simulated response corresponds to an over-damped system while the experimental response corresponds to an under-damped response (see Fig. 4).

The relationship between the virtual mass M_d and the damping ratio can easily be seen in (12). An increase in the virtual mass M_d reduces the damping ratio ζ. For a specific value of the mass — in this particular case $M_d = 35.37$ kg — the system shall become critically damped. In the experiments, however, the system becomes unstable as soon as the virtual mass is non-zero. Fig. 4 shows the experimental response for $M_d = 0$, $M_d = 0.5$ and $M_d = 1$. The discrepancy between the theoretical and experimental

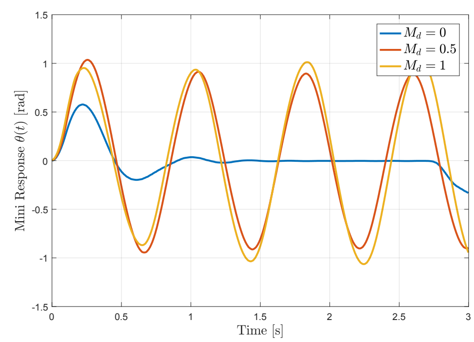

Fig. 4: Experimental response for different virtual mass M_d values. $\{K_d = 1000,\ C_d = 400\}$

response can be explained by several factors including noise in the measured signals, inaccurate parameters of the model and friction forces. In theory, a controller with only a stiffness gain K_d should not be stable. However experiments showed the response to be underdamped due to unmodeled friction at the mini mechanism joint (see Fig. 3).

Another difference is the response obtained when using a non-zero virtual mass M_d. In theory, the virtual mass M_d can be tuned in order to obtain a quicker response (i.e. reducing the damping ratio). However, the adjustment of this gain should be done carefully since it can make the controller underdamped.

With regards to the experimental results obtained with a non-zero virtual mass M_d, it can be observed that another option to obtain a lower damping ratio (i.e. faster response) is to increase the virtual stiffness K_d. On the other hand, only using a higher virtual stiffness ($K_d \geq 1000$) with the same damping ratio ($C_d = 400$) makes the system too sensitive to small position variation. For motion with large amplitude, the controller provides quick and rough response. However, the controller is too sensitive for fine and precise motion.

V. Frequency-Dependent Stiffness Controller

As described in the preceding section, using a nonzero virtual mass M_d in the impedance controller generates instability because of the small interaction of the passive mini mechanism and the noise level in the mini acceleration signal $\ddot{p}(t)$. A controller using the virtual damping and stiffness term provides stable control but lacks responsiveness, mostly for fine and precise motion.

Increasing the inertia of the mini mechanism could be an option to improve fine motion as it would filter the high-frequency motion of the operator. However this would mean that the operator will fatigue faster when using the system for longer periods.

Another means of emulating a small inertia in the controller is proposed here. It is shown in [14] that a delay in the admittance control generates an increase in perceived inertia by the user. While a too long delay makes the admittance controller impractical, a small delay in the controller could induce just enough virtual inertia to make the control effective. The same principle could be applied for an impedance controller.

It is proposed here to add a small delay on the position control term $p(t)$ by adding a virtual stiffness term K_f that is linked to a low-pass filtered version of $p(t)$. This means that the control will be more sensitive to low frequency motion, effectively reducing the system's response to high frequency motion such as trembling of the hand for fine motion. The cut-off frequency of the low-pass filter is chosen to render the control responsive in the human-arm bandwidth and reduce response to higher frequency motion like oscillations caused by human tremor. Hence the control shall be effective not only for large and imprecise motion but also for fine manipulation.

A. Controller Description

The controller presented here is based on the controller used in [6], except that the output is a force $F(t)$ instead of a desired velocity $\dot{x}_M(t)$. The force output $F(t)$ is transformed into a torque $\tau_M(t)$ using the right-hand side of (9) before being sent to the macro mechanism. The controller equation is shown below.

$$F(t) = C_d\dot{p}(t) + K_d p(t) + K_f p_f(t) \tag{15}$$

Herein, $p(t)$ represents the position of the mini mechanism along the x-axis and the term $p_f(t)$ represents a low-pass filtered version of this position $p(t)$. The term K_f is also representing a virtual stiffness. Again, (15) can easily be converted into the same form as (8) using the same angle approximation. This yields the following final control equation.

$$F(t) = lC_d\dot{\theta}(t) + lK_d\theta(t) + lK_f\theta_f(t) \tag{16}$$

The virtual stiffness terms K_d and K_f are used together because a response to high frequency motion is still desired. Only using the K_f term would completely eliminate the response to any motion above the cut-off frequency.

B. System Response

The stability of the alternative controller can be studied by substituting (5) into the controller equation (16) and taking the Laplace transform, which yields

$$\begin{aligned} F_H(s) \;&=\; \frac{m}{M+m}\Bigg[K_d l\Theta(s) + C_d ls\Theta(s) + K_f l\Theta_f(s) \\ &+\; (M+m)g\Theta(s) + Mls^2\Theta(s)\Bigg] \end{aligned} \tag{17}$$

The low-pass filtered $\Theta_f(s)$ can easily be related to $\Theta(s)$ in the Laplace domain via the low-pass filter transfer function where ω_c represents the low-pass cutoff angular frequency, namely

$$\Theta_f(s) = \frac{\omega_c}{s+\omega_c}\Theta(s). \tag{18}$$

Substituting (18) into (17) then yields

$$\frac{\Theta(s)}{F_H(s)} = \left[\frac{M+m}{mMl}\right]\frac{s+b_0}{a_3s^3+a_2s^2+a_1s+a_0} \tag{19}$$

with

$$\begin{aligned} b_0 &= \omega_c \\ a_0 &= \left(\frac{1}{M}\Big(K_d+K_f\Big) + \frac{g}{l}\Big(1+\frac{m}{M}\Big)\right)\omega_c \\ a_1 &= \frac{1}{M}\Big(K_d + C_d\omega_c\Big) + \frac{g}{l}\Big(1+\frac{m}{M}\Big) \\ a_2 &= \omega_c + \frac{C_d}{M} \\ a_3 &= 1 \end{aligned} \tag{20}$$

C. Stability Analysis

While the standard impedance controller was easily analyzed using the damping ratio ζ and angular cutoff frequency ω_0, the above system is more complex and such parameters cannot be used. Instead, the poles of the system defined from the roots of the denominator ($a_3s^3 + a_2s^2 + a_1s + a_0$) are used to predict the system response. Since the denominator is a cubic polynomial function, the roots, s_i, are found using the following equations.

$$\begin{aligned} \Delta &= 18a_3a_2a_1a_0 - 4a_2^3a_0 + a_2^2a_1^2 - 4a_3a_1^3 - 27a_3^2a_0^2 \\ \Delta_0 &= a_2^2 - 3a_3a_1 \\ \Delta_1 &= 2a_2^3 - 9a_3a_2a_1 + 27a_3^2a_0 \\ C &= \sqrt[3]{\frac{\Delta_1 \pm \sqrt{-27a_3^2\Delta}}{2}} \\ s_i &= -\frac{1}{3a_3}\left(a_2 + C + \frac{\Delta_0}{C}\right) \end{aligned} \tag{21}$$

The cubic discriminant Δ can be used to determine the nature of the system's response. Indeed, when $\Delta > 0$, the polynomial has 3 distinct real roots, hence the system is over-damped. When the discriminant $\Delta < 0$, then the polynomial has one real root and two complex conjugate roots, which means that the system is under-damped and will therefore oscillate around the equilibrium position. When the discriminant is equal to zero ($\Delta = 0$), then the polynomial's roots are all real and there is a multiple root. This case represents the critically damped system. For stability, all roots must have a negative real part.

Similarly to the case of the standard impedance controller, the objective is to be able to define one of the gains as a free variable that is used to compute the remaining gains in order to get a critically damped system. While a critically damped system is theoretically possible, in practice an over-damped system is better suited to reduce the probability of obtaining unstable behaviours.

1) Critically Damped System $\{\Delta = 0, \Delta_0 = 0\}$*:* For a critically damped system, the real roots must be identical (multiple root). This happens only when the two following conditions are met:

$$\Delta = 0, \text{ and } \Delta_0 = 0 \tag{22}$$

In that case, the multiple real root is defined by the following expression

$$s_i = -\frac{a_2}{3a_3} = -\frac{a_2}{3} \tag{23}$$

The system is stable if and only if the multiple root has a real negative value. Hence the following condition is found

$$a_2 > 0 \tag{24}$$

which corresponds to

$$C_d > -\omega_c M. \tag{25}$$

Since both constants $\{M, \omega_c\}$ have a positive value, the final condition is

$$C_d > 0. \tag{26}$$

Since a condition is defined for C_d, this gain will be used as a free variable to compute the remaining two gains $\{K_d, K_f\}$. A relation between K_d and C_d is found using the condition $\Delta_0 = 0$, which yields

$$K_d = \frac{1}{3}\left[\frac{C_d^2}{M} - C_d\omega_c + \omega_c^2 M - \frac{3g}{l}(M+m)\right] \tag{27}$$

An expression to obtain the gain K_f from C_d is found using the condition $\Delta = 0$.

$$K_f = \frac{1}{27}\left[\frac{-8\omega_c^3 M^3 + C_d^3 + 12C_d\omega_c^2 M^2 - 6C_d^2\omega_c M}{M^2\omega_c}\right] \tag{28}$$

2) Over-damped System $\{\Delta = 0, \Delta_0 \neq 0\}$*:* For the current system to be over-damped, all its poles must have real negative values, and more than one root is needed. This means that the cubic function discriminant must again meet the condition ($\Delta \geq 0$). For the sake of simplicity, we will use the condition $\Delta = 0$. In order to have more than one pole — difference with the critically damped system — the condition on Δ_0 becomes $\Delta_0 \neq 0$.

$$\begin{aligned} &\Delta_0 \neq 0 \\ &\Delta_0 = a_2^2 - 3a_1 \neq 0 \\ &a_2^2 \neq 3a_1 \end{aligned} \tag{29}$$

Using this first condition, the following expression for K_d is obtained

$$K_d \neq \frac{1}{3}\left[\frac{C_d^2}{M} - C_d\omega_c + \omega_c^2 M - \frac{3g}{l}(M+m)\right] \tag{30}$$

Now, looking at the poles s_1 and s_2 of the system, we have the following conditions for a stable system.

$$\begin{aligned} s_1 &= \frac{9a_0 - a_2 a_1}{2\Delta_0} < 0 \\ s_2 &= \frac{4a_2a_1 - 9a_0 - a_2^3}{\Delta_0} < 0 \end{aligned} \tag{31}$$

For the critically damped system, the evaluation of the single root was simple as it provides the stability limits of C_d. For the over-damped case, the problem is ill-posed since we have two inequalities with three variables $\{K_d, C_d, K_f\}$. Expressions for K_d and K_f as functions of C_d — such as the expression found for the critically damped system — cannot be obtained here. However, the provided conditions can be used to verify that the gains $\{K_d, C_d, K_f\}$ are in the stable region. The complete expressions from eq. 31 are readily obtained but are not included here because of space limitation.

3) Methodology: Even though no analytical solution was obtained to correctly set the gains to get an over-damped system, a methodology is proposed here that uses the relations obtained for the critically damped system. It is hypothesized here that an over-damped behaviour can be reached from a critically damped system by slightly modifying its gains. The same conditions are used to ensure stability. The first step is to set a strictly positive (non-zero) virtual damping value C_d. Then we get an expression for K_d using (27), but the virtual damping C_d is instead replaced with γC_d, where γ is a real coefficient, yielding

$$K_d = \frac{1}{3}\left[\frac{(\gamma C_d)^2}{M} - \gamma C_d\omega_c + \omega_c^2 M - \frac{3g}{l}(M+m)\right] \tag{32}$$

The condition $\Delta = 0$ is then used to get an expression for the remaining term K_f, which gives

$$\begin{aligned} K_f = \frac{1}{27M^2\omega_c}[&-8\omega_c^3 M^3 + 6\omega_c^2 M^2 C_d + 6\omega_c^2 M^2 \gamma C_d \\ &- 3\omega_c M C_d^2 \gamma + 3\omega_c M C_d^2 - 6\omega_c M \gamma^2 C_d^2 - 2C_d^3 \\ &+ 3\gamma^2 C_d^3 + 2\sqrt{-C_d^3(\gamma-1)^3(C_d\gamma + C_d - \omega_c M)^3}] \end{aligned} \tag{33}$$

If $\gamma = 1$, then (32) and (33) become respectively (27) and (28). The system would then be critically damped. Now only the coefficient γ needs to be defined in order to get an over-damped system. We therefore need to define a domain within which γ provides real negative roots. The roots (31) are readily obtained as a function of γ but the expressions are not given here because of space limitation.

Starting with the over-damped system condition, i.e., that the roots be real (not complex conjugates) simplifies the above mentioned conditions to

$$-C_d^3(\gamma-1)^3(C_d\gamma + C_d - \omega_c M)^3 > 0 \tag{34}$$

By definition, $C_d^3 > 0$, hence the previous inequality is true if and only if

$$\text{sign}[(\gamma - 1)^3)] \neq \text{sign}[(C_d\gamma + C_d - \omega_c M)^3] \tag{35}$$

From the left-hand side of (35), one has

$$\begin{aligned} (\gamma-1)^3 < 0 \text{ when } \gamma < 1 \\ (\gamma-1)^3 > 0 \text{ when } \gamma > 1 \end{aligned} \tag{36}$$

and from the right-hand side, one has

$$\begin{aligned} (C_d\gamma + C_d - \omega_c M)^3 < 0 \text{ when } \gamma < \frac{\omega_c M}{C_d} - 1 \\ (C_d\gamma + C_d - \omega_c M)^3 > 0 \text{ when } \gamma > \frac{\omega_c M}{C_d} - 1. \end{aligned} \tag{37}$$

Hence, the roots $\{s_1, s_2\}$ and the term K_f are real for the following domain of γ:

$$\begin{aligned} \left[\frac{\omega_c M}{C_d} - 1 < \gamma < \ 1\right] \text{ if } \left(\frac{\omega_c M}{C_d} < 2\right) \\ \left[1 < \gamma < \frac{\omega_c M}{C_d} - 1\right] \text{ if } \left(\frac{\omega_c M}{C_d} > 2\right) \end{aligned} \tag{38}$$

Equation (38) provides a bounded domain within which the roots are real and where the solution might be an over-damped system. It is proposed to start from $\gamma = 1$ and either slowly increase (or decrease) its value.

While it does not give a proven γ domain for which the system is over-damped, it proposes a bounded trial-and-error method with a clear starting point ($\gamma = 1$) which comes from physical insight (i.e. critically damped system). The methodology can be stated as follows:

1) Select a strictly positive real virtual damping value $C_d > 0$.
2) Compute the boundary for γ using (38).
3) Starting from $\gamma = 1$, either increase of decrease γ depending on its previously computed domain. Compute the roots $\{x_1, x_2\}$ and verify that they are negative.
4) Compute the gains K_p and K_f using (32) and (33) respectively.
5) Compute the system response $\theta(t)$ using (19). If the response is satisfactory (sufficiently over damped), then select the computed gains $\{C_d, K_d, K_f\}$.

4) Example: The current example uses the experimental parameters of the set-up described in Section II. The virtual damping is selected to be $C_d = 400$ kg/s and the frequency $\omega_c = 100$ rad/s. The boundaries of γ are initially computed using (38).

$$\frac{\omega_c M}{C_d} = 0.35 \tag{39}$$

$$-0.65 < \gamma < 1 \tag{40}$$

Fig. 5 shows the simulated response for several values of γ in this range. The relation between γ and the type of response is observed. First, it is noted that the responses obtained when using the boundary values of the coefficient (in this case $\gamma = -0.65$ and $\gamma = 1$) are identical, i.e. a critically damped response.

The response obtained at the centre of the coefficient domain ($\gamma = 0.175$) is the most damped. As the value of the coefficient gets closer to one of the boundaries, the response obtained gets closer to the critically damped response. The system response was also computed for $\gamma = 1.5$, which is outside the damped boundary. For this value of γ, the response is indeed underdamped.

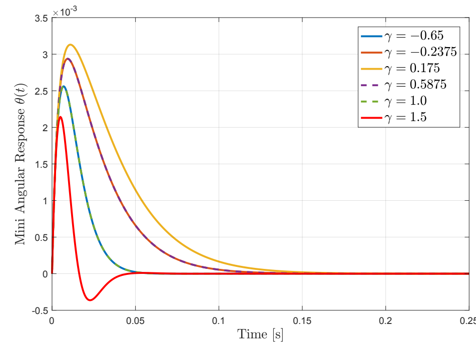

Fig. 5: Simulated response of the system for different values of γ using the proposed methodology for an over-damped system gain sets.

D. Experimental Stability Analysis

As already explained in Section IV, the discrepancies between the theoretical model and the experimental setup force us to use an empirical methodology to set stable gains. When the virtual stiffness K_f is equal to zero, the system reverts back to the standard impedance controller with a zero virtual mass ($M_d = 0$). Therefore, the same value of virtual stiffness ($K_d = 1000$) and virtual damping ($C_d = 400$) previously found can be used safely again, only the virtual stiffness K_f needs to be determined. As stated before, increasing the response in position — by adding the term K_f in the controller — should reduce the original damping ratio of the standard impedance.

The same gain values used for the standard impedance controller were tried here for the new frequency-dependent stiffness gain K_f. The results obtained are shown in Fig. 6. Compared with the virtual mass M_d term of the standard impedance controller, the new virtual stiffness term K_d provides a stable response to external perturbations.

The system responses retain the same form for any value of K_f that was tested. Increasing the new virtual stiffness K_f provides a slightly faster response to perturbation. From Fig. 6, the best response could subjectively be selected to be $K_f = 500$ since it provides a quicker response without increasing the oscillation significantly. Using the combination of virtual stiffness $\{K_d = 1000,\ K_f = 500\}$ means that manipulation with a motion frequency below ω_c should have a 50% higher response than for higher frequency motion.

While this is not apparent on the graphs, the system response feels more intuitive with the new virtual stiffness term K_f. The system is more responsive to standard motion amplitude and frequency while effectively reducing the high frequency motion such as hand trembling.

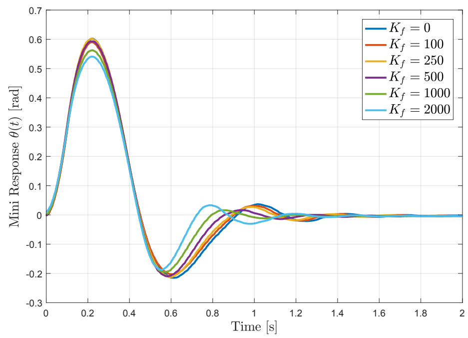

Fig. 6: Experimental response for different values of frequency-dependent virtual stiffness K_f. $\{K_d = 1000, C_d = 400\}$

E. Discussion

An alternative impedance controller was presented here for an active-macro/passive-mini robotic system in order to solve the instability problem of the standard impedance control when using a non-zero virtual mass M_d. The new controller uses an additional stiffness term that is linked to a filtered (low-pass) position signal $p(t)$. The proposed alternative controller provides a quick and stable response, both for large amplitude and precise motions. Experimental results showed that stability is not an issue, even for high values of stiffness. The theoretical analysis was more complex than for the standard impedance controller since the transfer function of the system has an additional pole. In other words, the system is no longer a classical second-order low-pass filter and hence cannot be analyzed solely using a damping ratio ζ and a cutoff frequency ω_0. A methodology was nevertheless provided in order to safely go from a critically damped system to an over-damped system, using a mathematical analysis of the transfer function. It could be argued that only the filtered virtual stiffness K_f could be used (with the virtual damping C_d). However the original virtual stiffness K_d gain provides a baseline response in position for both low and high-frequency motion. This baseline gain yields an effective control.

VI. Conclusion

In this paper, two different impedance controllers were presented. Each of the controllers was theoretically and experimentally analysed. The first controller consists of the standard impedance control firstly described in [7], consisting of a virtual mass M_d, damping C_d and stiffness K_d. The stability of the system in response to a unit-impulse force $f_h(t)$ was presented. Comparison between the theoretical and experimental responses showed discrepancies between the experimental setup and the model. Stable responses were obtained when using the terms C_d and K_d. However, the use of a nonzero virtual mass M_d causes the system to become unstable. In order to address the stability issue related to the virtual mass M_d of the standard impedance controller, this term was replaced by another virtual stiffness term K_f which is linked to a low-pass version of the position of the mini mechanism $\theta_f(t)$. Using the low-pass term $K_f\theta_f(t)$ generates a small delay in the stiffness term that is felt by the user as a simulated inertia. The theoretical stability of such a controller was presented. An analytical expression to obtain a critically damped system was found and a methodology was proposed to safely go from a critically damped system to an over-damped system. Experimental results demonstrated that the replacement of the term $M_d\ddot{\theta}(t)$ by $K_f\theta_f(t)$ solves the instability problem and helps to reduce high-frequency motion such as hand tremor. This additional virtual inertia helps for fine and precise motion that is affected by the human tremor. The approach can be extended to systems with mutiple degrees of freedom, even though it may not be possible to obtain analytical expressions in such cases.

References

[1] T. S. Tadele, T. de Vries, and S. Stramigioli, "The safety of domestic robotics: A survey of various safety-related publications," *IEEE robotics & automation magazine*, vol. 21, no. 3, pp. 134–142, 2014.

[2] J. Krüger, T. K. Lien, and A. Verl, "Cooperation of human and machines in assembly lines," *CIRP annals*, vol. 58, no. 2, pp. 628–646, 2009.

[3] A. Cherubini, R. Passama, A. Crosnier, A. Lasnier, and P. Fraisse, "Collaborative manufacturing with physical human–robot interaction," *Robotics and Computer-Integrated Manufacturing*, vol. 40, pp. 1–13, 2016.

[4] P. D. Labrecque, J.-M. Haché, M. Abdallah, and C. Gosselin, "Low-impedance physical human-robot interaction using an active–passive dynamics decoupling," *IEEE Robotics and Automation Letters*, vol. 1, no. 2, pp. 938–945, 2016.

[5] P. D. Labrecque, T. Laliberté, S. Foucault, M. E. Abdallah, and C. Gosselin, "Uman: A low-impedance manipulator for human–robot cooperation based on underactuated redundancy," *IEEE/ASME Transactions on Mechatronics*, vol. 22, no. 3, pp. 1401–1411, 2017.

[6] N. Badeau, C. Gosselin, S. Foucault, T. Laliberté, and M. E. Abdallah, "Intuitive physical human-robot interaction: Using a passive parallel mechanism," *IEEE Robotics & Automation Magazine*, vol. 25, no. 2, pp. 28–38, 2018.

[7] N. Hogan, "Impedance control: An approach to manipulation," in *1984 American control conference*. IEEE, 1984, pp. 304–313.

[8] A. Lecours, B. Mayer-St-Onge, and C. Gosselin, "Variable admittance control of a four-degree-of-freedom intelligent assist device," in *2012 IEEE International Conference on Robotics and Automation*. IEEE, 2012, pp. 3903–3908.

[9] W. S. Newman and Y. Zhang, "Stable interaction control and coulomb friction compensation using natural admittance control," *Journal of robotic systems*, vol. 11, no. 1, pp. 3–11, 1994.

[10] S. P. Buerger and N. Hogan, "Complementary stability and loop shaping for improved human–robot interaction," *IEEE Transactions on Robotics*, vol. 23, no. 2, pp. 232–244, 2007.

[11] E. Colgate and N. Hogan, "An analysis of contact instability in terms of passive physical equivalents," in *Proceedings, 1989 international conference on robotics and automation*. IEEE, 1989, pp. 404–409.

[12] X. Lamy, F. Colledani, F. Geffard, Y. Measson, and G. Morel, "Achieving efficient and stable comanipulation through adaptation to changes in human arm impedance," in *2009 IEEE International Conference on Robotics and Automation*. IEEE, 2009, pp. 265–271.

[13] J. E. Colgate and N. Hogan, "Robust control of dynamically interacting systems," *International journal of Control*, vol. 48, no. 1, pp. 65–88, 1988.

[14] I. A. Kuling, J. B. Smeets, P. Lammertse, B. Onneweer, and W. Mugge, "Delays in admittance-controlled haptic devices make simulated masses feel heavier," *PloS one*, vol. 10, no. 9, p. e0138023, 2015.